

ARTIFICIAL NEURAL NETWORKS FOR IMPROVED IMAGE RECONSTRUCTION IN ELECTRICAL IMPEDANCE TOMOGRAPHY

Fakhar Anjam¹, Najib Ur Rehman², Muhammad Atif Imtiaz³, Muhammad Uzair⁴, Sumaira Imtiaz⁵, Wahab Khan⁶, Laiba Gul⁷, Javed Khan Marwat⁸, Ali Mujtaba Durrani⁹

¹Department of Electrical Engineering, University of Science & Technology, Bannu, Pakistan

²University of Girona,

³Polytechnic Institute Australia; Faculty of Electronics and Electrical Engineering, University of Engineering and Technology, Taxila, Pakistan

⁴Department of Computer Science, National University of Computer and Emerging Sciences, Islamabad, Pakistan

⁵Department of Computer Science, The Millennium Universal College, Peshawar, Pakistan

⁶Department of Electrical Engineering, University of Science and Technology Bannu

⁷Department of Computer Science, National University of Computer and Emerging Sciences, Islamabad, Pakistan

⁸Senior Engineer, Material Management, PESCO, Peshawar Electric Supply Company, Peshawar, Pakistan.

⁹Department of Electrical Engineering, CECOS University of IT and Emerging Sciences, Peshawar, Pakistan.

¹f.anjam@ustb.edu.pk, ²syed.najib@udg.edu, ³imtiaz.matif@gmail.com, ⁴muhammaduzair98@gmail.com,

⁵sumaira.imtiaz@tmuc.edu.pk, ⁶wahab487@yahoo.com, ⁷laibalg6117@gmail.com, ⁸enr.jade@gmail.com,

⁹ali@cecos.edu.pk

DOI: <https://doi.org/10.5281/zenodo.15349107>

Keywords

EIT, ANN, Image Reconstruction, EIDORS, Neural Network

Article History

Received on 28 March 2025

Accepted on 28 April 2025

Published on 06 May 2025

Copyright @Author

Corresponding Author: *

Ali Mujtaba Durrani

Abstract

The research applies the Artificial Neural Network (ANN) method to create images by utilizing Electrical Impedance Tomography (EIT) as its image reconstruction system. The ANN technique demonstrates versatility because its applications extend across different domains, which include classification functions with additional enhancement capabilities and reconstruction procedures. Data receives classifications in multiple domains according to its purpose, where numbers or animals, or signboards represent three examples of categorized data. The enhancement technique functions to both enhance the image quality and remove unwanted noise, and it operates either on 1-D data alone or on 2-D data based on user needs. The image reconstruction process requires both the input and output neurons of the neural network to have the same number for accurate image reconstruction. The technique supports application to signals of 1-D, 2-D, and 3-D dimensions that generate outcome vectors or matrices of identical sizes to the input data. The research implements an ANN to restore visual information from the source data.

The document follows a standard organization with chapters starting from the introduction to methods through results before concluding. The first part of the paper delivers a technique summary along with research reviews related to multiple uses of neural networks. The proposed approach receives a detailed explanation throughout the methods part, followed by a result presentation of images before and after the neural network technique usage. The final chapter brings together the conclusions based on the released results, which point toward

INTRODUCTION

The research employs an artificial neural network (ANN) as a neural network (NN) reconstruction technique to restore images. The ANN technique exists as a data reconstruction method that operates with pre-processed and raw data. Researchers generated their training and testing dataset through EIDORS simulation-based software (Electrical Impedance Tomography and Diffuse Optical Tomography Reconstruction Software) [1]. The electrical impedance tomography (EIT) method operates as Industrial Tomography Systems (ITOMS or simply ITS) for visual detection by employing tomography and computed tomography (CT) scanner principles. The two techniques use equivalent principles of operation in their functionality [2]. Real-time and offline images from the EIT procedure result from electric current transmission at defined frequencies through electrode pairs for industrial and biomedical applications. The obtained signals lead to extrapolated values that create the images. The visual representations generated from these images enable the study of solution mixing and crystallization, together with biomedical problems, as well as bubble detection procedures. The tomographic procedures CT and IT, along with RT, represent prevalent formats among various tomography techniques [3]. The methods find use in multiple fields such as industrial and medical applications, and real-life detection of welding bubbles and imaging for

impedance tomography and analysis of the lungs [4]. The technology enables the processing of insulating surfaces through the examination of electrical permittivity (EP). For classification purposes, the artificial neural network (ANN) stands as a traditional technique [5]. The research employs this technique for the reconstruction of images that belong to electrical impedance tomography (EIT) systems. The neural network (NN) consists of input and output neurons [6]. A neuron, the basic cell in the brain, includes dendrites, an axon, an axon terminal button, a nucleus, a soma (cell body), and a myelin sheath, as shown in Figure 1. (a) [7]. A biological neuron equivalent model is constructed with input signals (dendrites), weights, an activation function, and output, as depicted in Figure 1.1(b) [8, 9]. Here, $x_1, x_2, x_3, \dots, x_n$ represent the inputs, $w_1, w_2, w_3, \dots, w_n$ are the weights, b_1, b_2, \dots, b_n are the biases, the activation function is denoted as $f(\cdot)$, and y represents the output of the neural network [10]. There are various types of neural networks used for different applications, including classification, reconstruction, and enhancement [11-13]. Classification involves a greater number of input neurons than output neurons (Figure 2). In the reconstruction technique, the number of input neurons equals the number of output neurons (Figure 3). At the same time, enhancement involves a smaller number of neurons in the input layer than in the output layer (Figure 4).

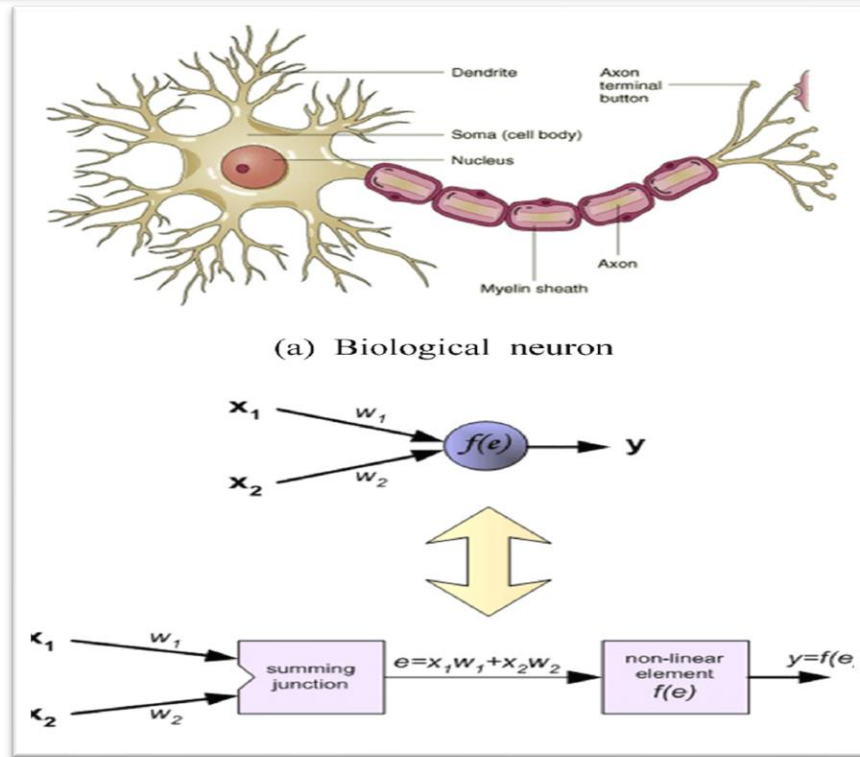


Figure Error! No text of specified style in document..This is the biological neuron (b) is the equivalent model of the biological neuron [15]

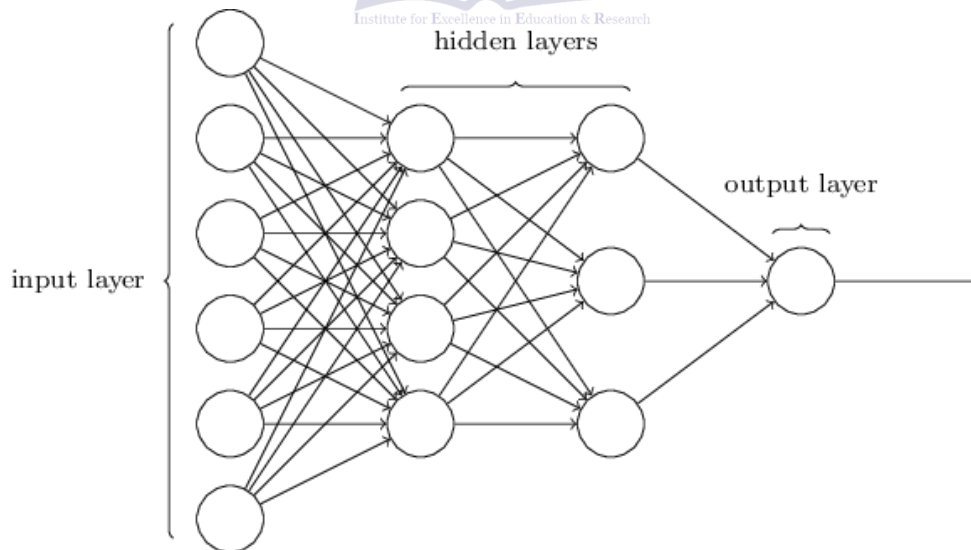


Figure 1 Classification neural network structure [14]

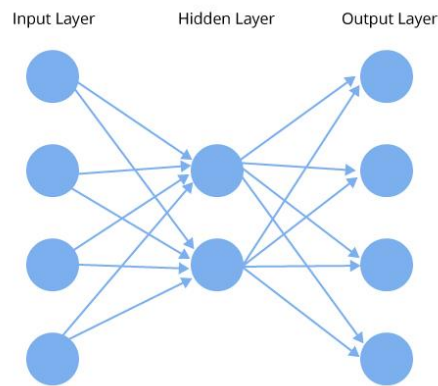


Figure 2. Reconstruction of neural network structure [15]

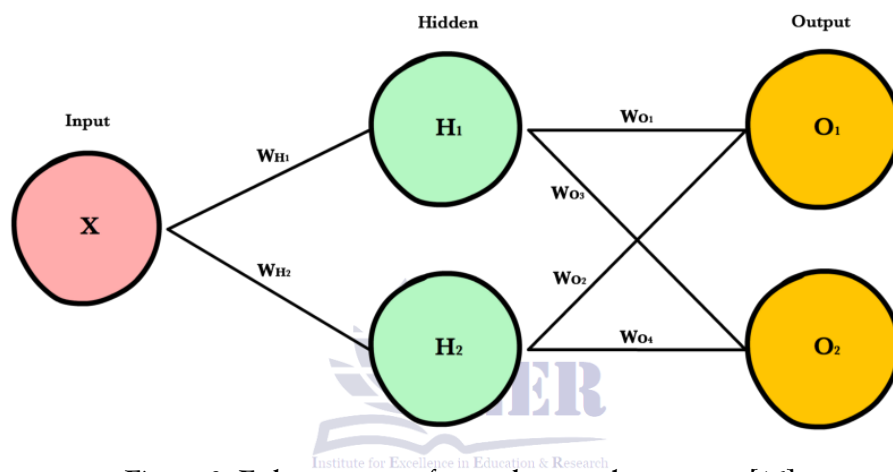


Figure 3. Enhancement of neural network structure [16]

The activation function is a critical component in a neural network system as it triggers the output when a threshold value is reached [17]. Once this threshold is surpassed, the neuron will be activated. The sigmoid activation function is one of the most widely used in neural networks, with other activation functions shown in Figure 1-5 [18]. The sigmoid function maps input values, denoted as z , to an output that ranges from 0 to 1. As the input value approaches negative infinity, the output tends toward zero, and as the input approaches positive infinity, the output approaches one. The unit step activation function, also known as the Heaviside or binary activation function [20], is triggered at two levels, providing a binary output: 0 for inputs below a threshold and 1 for inputs above the threshold. This function is shown in Figure 1.6. The Heaviside function can be mathematically represented as $\varphi(z) = 0$ for $z < 0$ and $\varphi(z) = 1$ for $z \geq 0$ [21]. Another

activation function is the sign function, represented by $\varphi(z) = -1$ for $z < 0$, $\varphi(z) = 0$ for $z = 0$, and $\varphi(z) = 1$ for $z > 0$, which has three possible output values [20]. The linear function, $\varphi(z) = z$, is another activation function that returns the same value as the input. The sigmoid function is represented as $\varphi(z) = 1/(1 + e^{-(z)})$ and is frequently used to produce outputs between 0 and 1, with values close to 0 for negative inputs and values close to 1 for positive inputs. The hyperbolic function, $\varphi(z) = (e^z - e^{-z}) / (e^z + e^{-z})$, and the ReLU (Rectified Linear Unit) function, $\varphi(z) = \max(0, z)$, are also used as activation functions in neural networks for various applications.

1. Literature

A researcher has developed a phantom equivalent model for the lungs and heart using a saline solution in the system [22]. This phantom, with inner electrodes, is used to flow electric current and create

images through electrical impedance tomography (EIT). Other researchers have worked on similar systems, but based on simulations, where they generated EIT images incorporating conductivity and permittivity [3]. While neural network techniques are widely used in image reconstruction, some studies have also applied different methods, such as the D-bar method for image reconstruction [23]. Research focused on two-dimensional (2D) images has involved clearing the phantom system and examining results using circular and triangular-shaped objects [24]. The authors demonstrated NN-SDM technology using a neural network-based supervised descent method to process online and offline dataset information in their research [25]. The neural network training process uses offline data to develop the network that subsequently runs within the online system for image reconstruction.

There exists a challenge to define the degree of knowledge in two-dimensional (2D) imaging systems, yet this approach delivers workable experimental outcomes. Three-dimensional (3D) models provide a comprehensive examination of information, which enables researchers to better explain the problems they encounter [26]. Medical experts used a 3D model to research breast tumors by presenting a simulated comparison of normal versus cancerous breast tissue [26]. Systems supply resistivity along with conductivity data that permits the construction of these 3D models [27]. A research paper combined two-dimensional and three-dimensional modeling to study system conductivity distribution by developing 3D structures using total variation for analysis purposes [27]. With a similar application, scientists use this methodology to investigate different types of physiological tissues present inside bodily organs. This approach enables medical examinations without requiring invasive surgical procedures because it remains non-invasive. The creation of a human body 3D model from a 64-electrode dataset was possible after a team conducted the research [28].

Researchers can utilize the Electrical Impedance Tomography and Diffuse Optical Reconstruction Software (EIDORS) to produce sample images that become suitable for creating ideal targeted specimens. Researchers easily manage EIDORS software through its freeware basis since they can change its structure for their convenience [1]. The

inverse problem software solves mathematical models to create target images as well as reconstructed images [1]. The combination of MATLAB and EIDORS enables users to solve forward and inverse problems to generate multiple 2D images that appear as a mesh in a two-dimensional format. A number of researchers have documented the mathematical algorithms used in these methods [29].

EIDORS has multiple versions, each updated with improved algorithms [30], and version 3.9 was used in this research. This software uses an equivalent model to create images for the phantom system, where the current and voltage measurements give information on resistivity and conductivity. A very low current is applied to the phantom body to collect voltage and current data at the system boundaries [31].

Image reconstruction is the process of creating images from raw or noisy data, which can often be distorted or affected by artifacts. High-resolution images are particularly important for examining the details of each pixel for data extraction [32]. High resolution ensures a dense pixel distribution near the targeted domain in the image, providing detailed information. In medical imaging, such detail is essential [33]. Conventional methods use filters and other techniques to extract features from images [34], but for better results, artificial intelligence and neural network techniques are used to create more detailed images [35, 36]. Standard methods may alias or subsample images, thereby eliminating important details. Still, neural networks can help convert low-resolution (LR) images into high-resolution (HR) images, which are crucial for medical applications. The analysis of the Region of Interest (ROI) remains difficult using low-resolution images, according to [37]. High-resolution images serve essential purposes in real-life CCTV cameras and surveillance systems, according to [38].

Neural network technology, which improves images built through EIDORS, finds common use in medical imaging for enhancing image quality [40]. The Region of Interest (ROI) enhancement process demands detailed, precise imaging techniques that neural networks help generate high-resolution images required for medical investigations. Artificial networks serve as tools that create image maps [41]. Multiple techniques based on neural networks have

been used for image reconstruction and enhancement through the Combination of Classification Neural Networks (CNN) and Artificial Neural Networks (ANN), and Deep Classification Neural Networks (DCNN), and Denoising Auto Encoder Networks (DAN) [42-46].

I have described my research methods, which encompass Electrical Impedance Tomography (EIT) alongside Electrical Impedance Tomography and Diffuse Optical Reconstruction Software (EIDORS). These methods encompass two-dimensional (2D) and three-dimensional (3D) imaging with both reconstruction and enhancement processes.

2. Methodology

The first step of this research is data collection. Electrical impedance tomography (EIT) and Diffuse Optical Tomography Reconstruction Software (EIDORS) are used in this research to generate the electrical impedance tomography (EIT) dataset. [47-49]. This is freeware software and it uses the finite element method (FEM) to generate the dataset. [50, 51]. The finite element method (FEM) model image is shown in Figure 5. [52]The data set was created using two solvers, one absolute and the other a difference solver. [53]. Two solvers are used to reconstruct the image, nodal and mesh, in

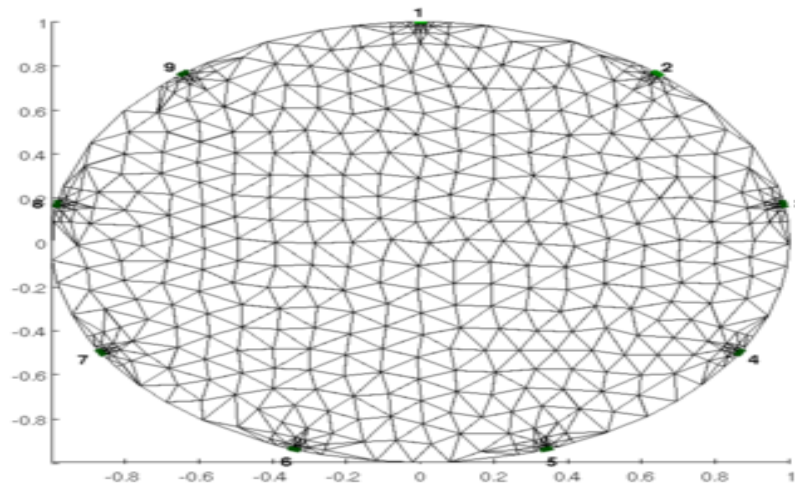


Figure 5. 8 Electrode FEM 2D model

This research mesh solver technique has been used to reconstruct the image in the FEM model. [54, 55]Intensive work can be extended to 2D and 3D

models; in this work, a 2D model is used. [56, 57], as shown in Figure 6.

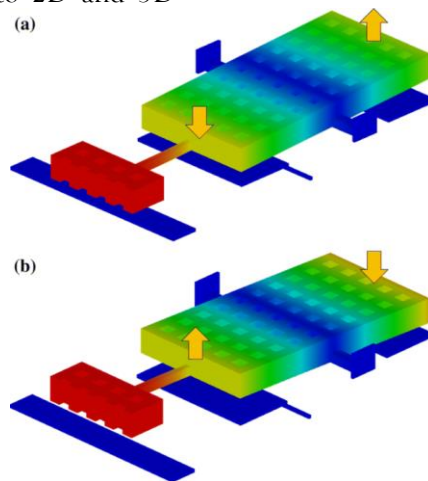


Figure 6. 16 Electrode FEM 3D model [58]

Electrical Impedance Tomography and Diffuse Optical Tomography Reconstruction Software (EIDORS) is a simulation-based freeware software. It uses the finite element method (FEM) to reconstruct the image from the voltages and current. The main key to rebuilding the target is in the conductivity or resistivity changes in the body when the current is applied at certain low voltages. [59]The applied

current at different electrodes is measured at different points around the body. This system has various combinations of electrodes. The most workable systems can be 8, 16, 32, 64, or 128-electrode systems. In this research, a 16-electrode phantom body (Figure 7) is used to collect the simulation-based signal (16 electrodes).

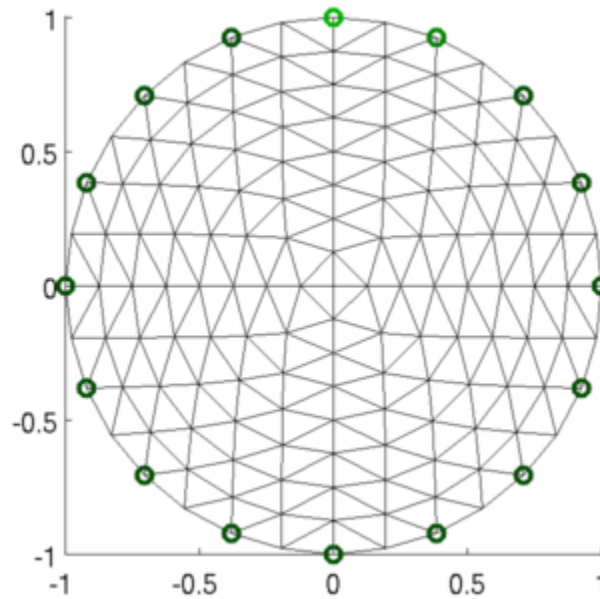


Figure 7. 16 Electrode FEM 2D model with meshes and conductivity scale [60]

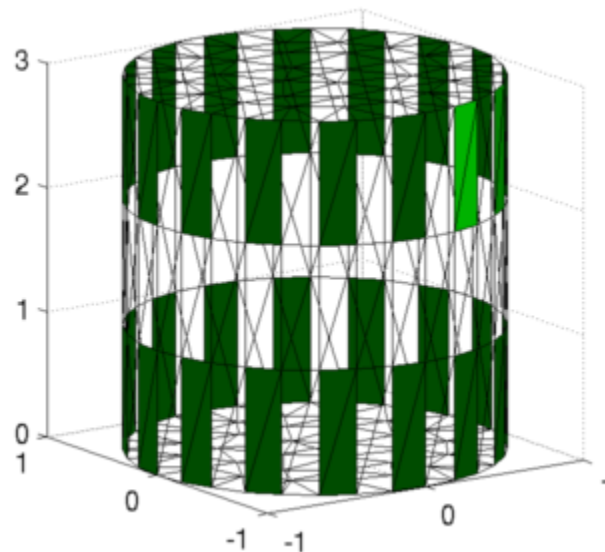


Figure 8. Meshes and Node

The finite element method (FEM) model is based on nodal or meshes networking with a different number of nodes and meshes inside the phantom area. Electrodes position defines the nodal position and, in the finite element method (FEM), meshes are the position of the phantom system starting from one in the middle of the system. The Mesh system used in this system is 1600, which makes the system robust enough to reconstruct the image with enough target detail. (Mesh and node Figure 3.4) Current collected from the phantom contains noise and needs to be removed. To remove the noises and artifacts,

different filters and methods are used. The Gaussian noise (GN) removal technique has been used in this research to remove the signal noise [61]. Noises can emerge from the phantom saline water distortion, electrode movements on the phantom body or the human body, or any other reason, like wire movement, etc. Phantom saline water also produces some noises and needs to be subtracted at the start of the experiment with an empty phantom object. (Noise Signal Figure 9)

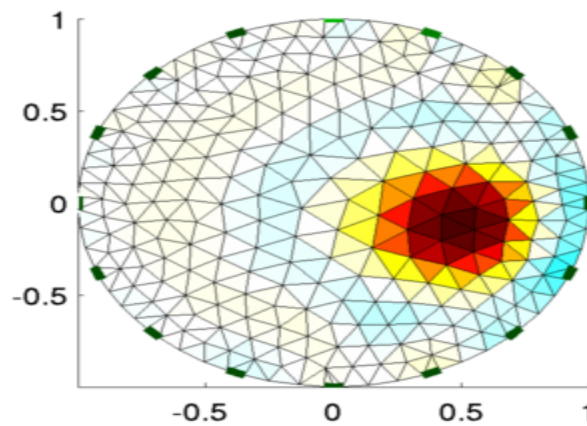


Figure 9. Target inside the FEM 2D model [48]

The Fast Fourier Transform (FFT) helps to analyze the signal features with different frequency

spectrums. [62]. There are different frequency spectrums in the recorded signal (Figure 10). [63]

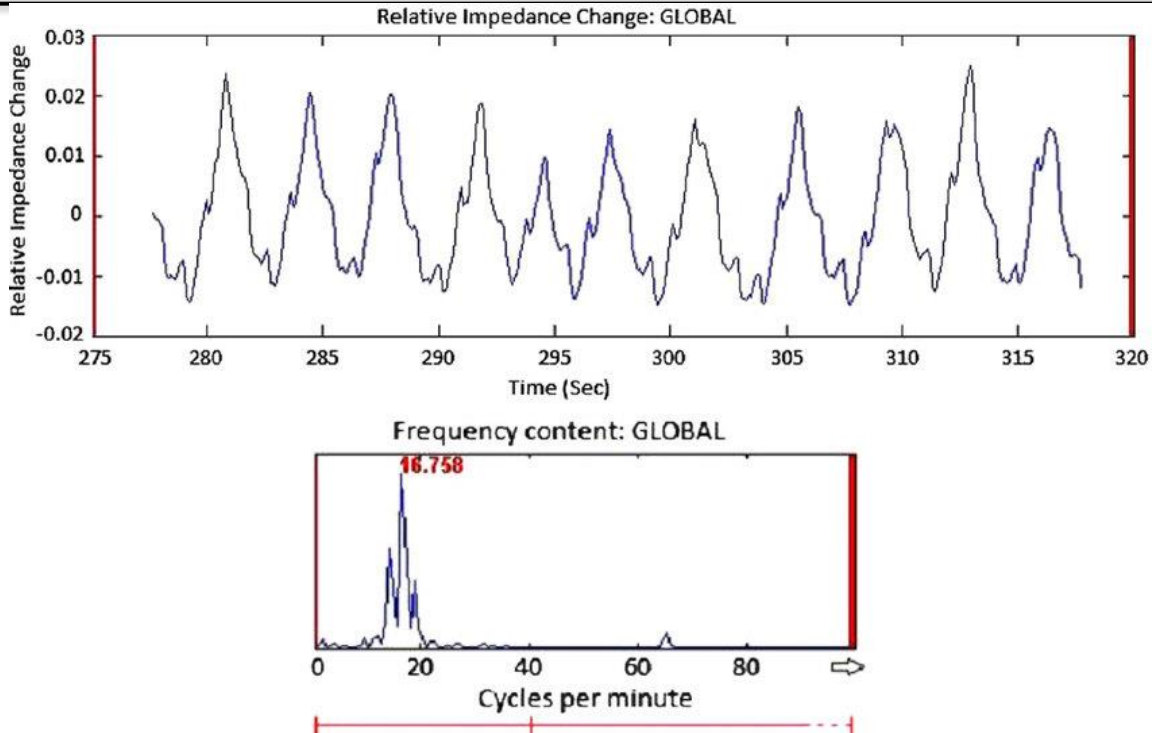


Figure 10. FFT of the EIT signal [63]

The neural network (NN) Mat lab toolbox is used to apply the neural network technique to the signal to reconstruct the image after the finite element method (FEM) model is applied [64, 65]. An artificial neural network (ANN) is a neural network

(NN) technology that can be used to classify, reconstruct, or enhance the signal. In this research, I have used the artificial neural network (ANN) technique to rebuild the image. (ANN Figure 11) [66].

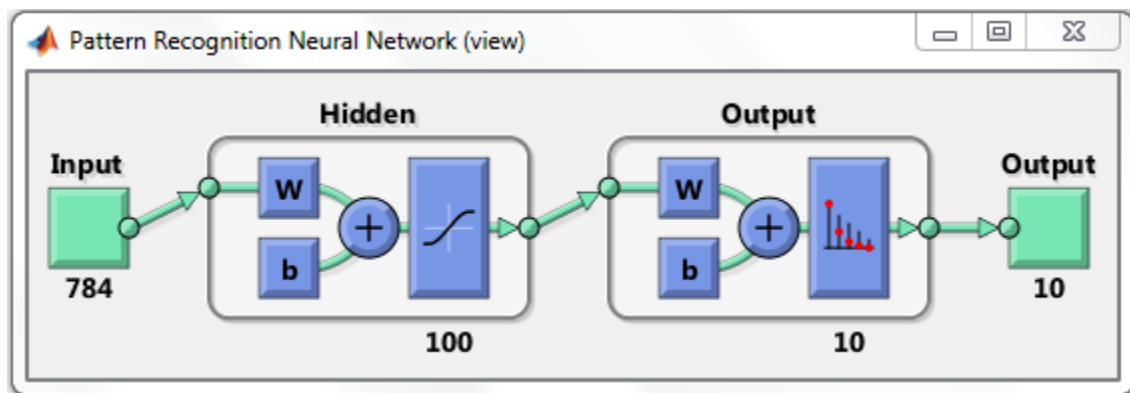


Figure 11: ANN in MATLAB with 784 input and 10 output neurons, 100 hidden neurons [66]

Finite element method (FEM) model in electrical impedance tomography and diffuse optical reconstruction software (EIDORS) creates the image that contains noises. That image is fed to the artificial neural network (ANN) for reconstruction. This image can be filtered or non-filtered. For the

filtered image neural network needs to be trained base on the filtered signal, and for the non-filtered signal, we need to train the non-filtered signal. (Filtered and non-filtered signal, Figure 11) Neural network training and testing are the phases when the neural network needs to be examined. The

mean square error (MSE) technique is used to analyze the system's error. [67].

Mean Square Error

$$MSE = \frac{1}{n} \sum_{i=1}^n (Y_i - y_i)^2 \tag{1}$$

Mean square error (MSE) is taken between the artificial neural network (ANN) resultant signal and

the original signal or the targeted signal. MSE is used to update the system's weights, which are updated during the neural network's training. In neural network techniques, there are input neurons, weights, bias, activation function, alpha, output neurons, and MSE. [68-70]. (Figure 12)

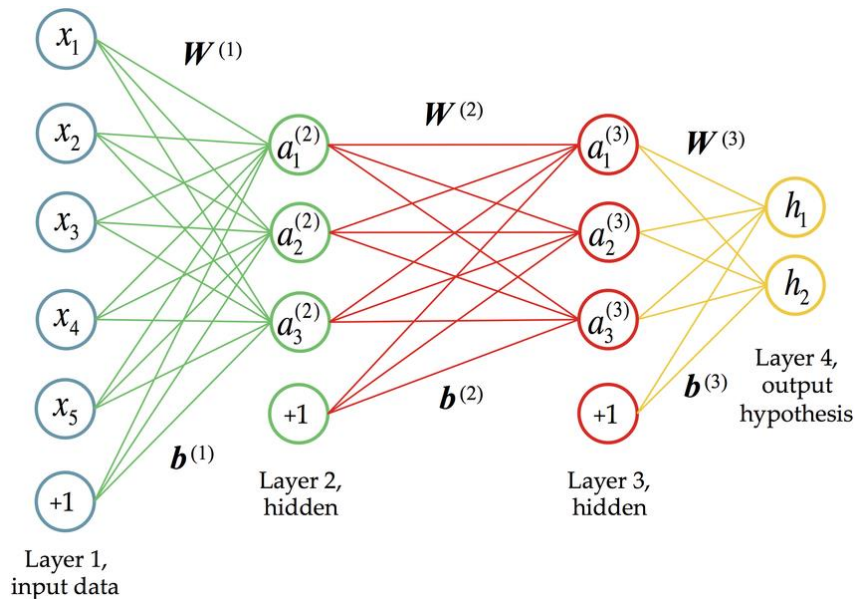


Figure 12. Basic NN with input x, a as the hidden neurons, w are the weights, and b is the bias [71]

Institute for Excellence in Education & Research

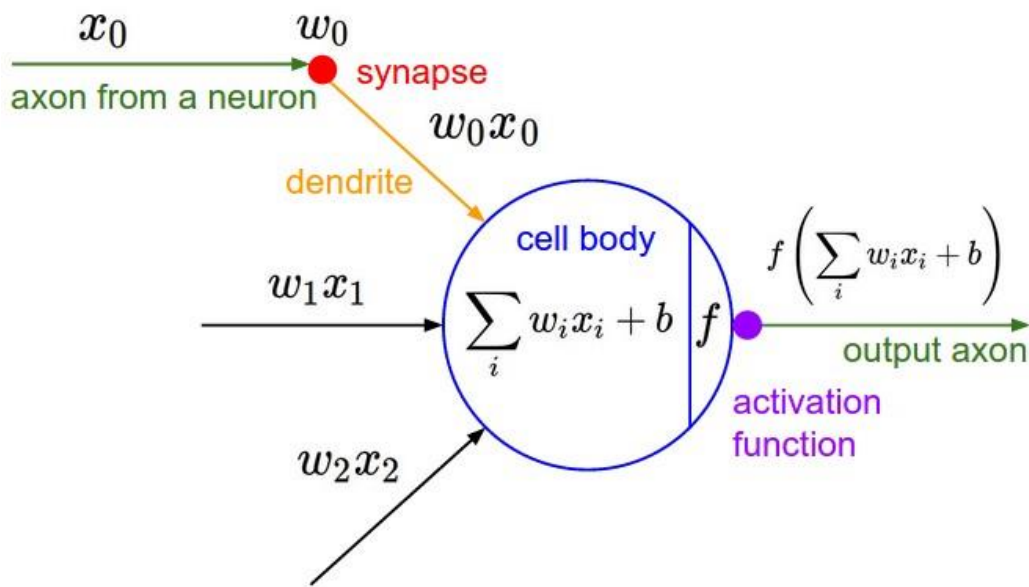


Figure 13. Single NN layer [71]

There are two phases, the training phase, and the testing phase. In the training phase, more data needs from the collected data. In this research 4000 data samples are collected of which 70% were used for

the training purpose and 30% for the testing phase. The sigmoid function is used for the activation function. (Data sample images Figure 14) [72]

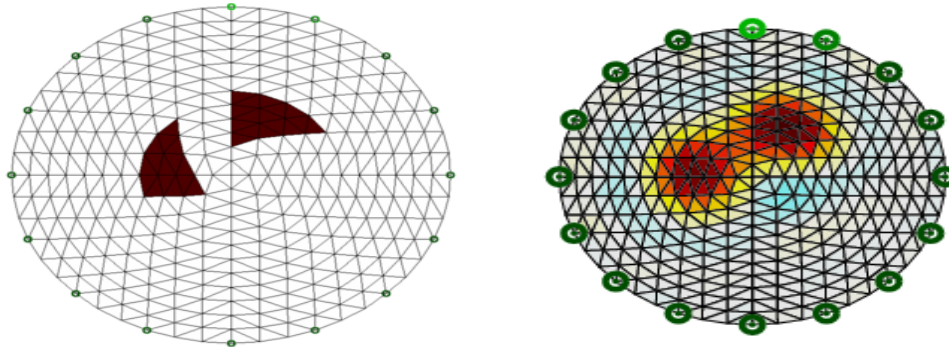


Figure 14. Two targets FEM, Left Is the ideal target and right is the reconstructed targets

Input and the output neurons take and produce the output signal respectively. The number of Input neurons can be changed to the number of pixels in the image or the signal samples at a specific time. Similarly, the output neurons can be changed to specific numbers based on the application. In the reconstruction techniques, the input and the output neurons are the same in size. Bias is the number that is added to the signal after the activation function is applied. The sigmoid activation function has been used in this research with a fixed bias. The bias value can be changeable or fixed. If the values variate from the reference point then the bias value should be variable otherwise it can be fixed. The activation function is shown in Figure 14.

Weights are updated after the calculation of the errors. Alpha (α) is the learning rate and is used to update the weights. Alpha should be selected carefully to control the weights' learning. If alpha is too small, learning will be slow. If alpha is too large,

learning can oscillate and cannot make the error MSE zero (Alpha Eq.).

$$W_x^* = W_x - \alpha \left(\frac{\partial \text{error}}{\partial W_x} \right) \quad (2)$$

3. Results

The results of the image reconstruction process will be presented, comparing the images before and after the application of the neural network. The image reconstruction technique employs an equal number of input and output neurons. The results of the neural network reconstruction are validated through comparison with the forward reconstruction method. During the training phase, input images are fed into the input neurons of the neural network, while the corresponding targeted images are provided at the output neurons. This process trains the neural network module to map the inputs to the desired outputs. The training and resulting reconstructions are visualized and discussed, as illustrated in Figure 15.

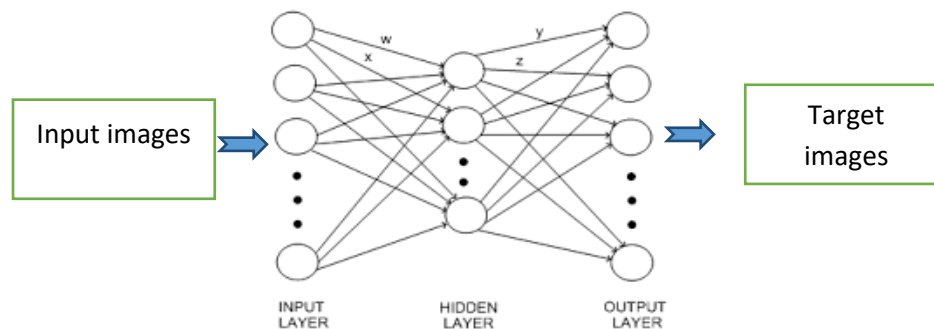


Figure 15. Training NN frame for the input and output neurons

The hidden layers in a neural network can be either single or multi-layered, depending on the complexity of the application and the problem being addressed. In this research, a single hidden layer with the sigmoid activation function has been utilized. A total of 4000 images were used for both training and

testing the neural network. After completing the training phase, the model is tested using a separate set of images that were not part of the training dataset. The results of the testing phase are shown in Figure 16.

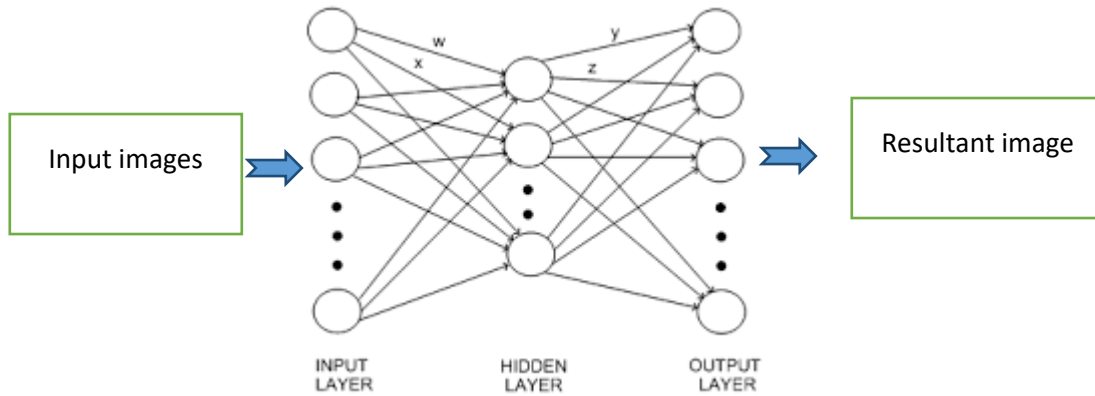


Figure 16. Testing NN with input and the output neurons

The resultant image is the image reconstructed from the neural network. The image that feeds to the input layers are shown in Figure 17.

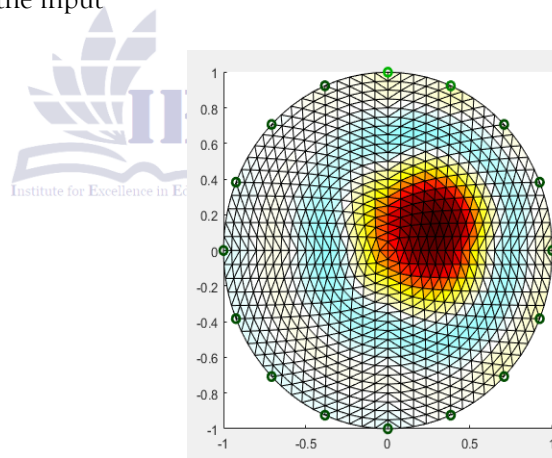


Figure 17. Target at different location, left image

target at the right bottom, left image target at the right upper near to center The zoom version of the reconstructed image is shown in Figure 18.

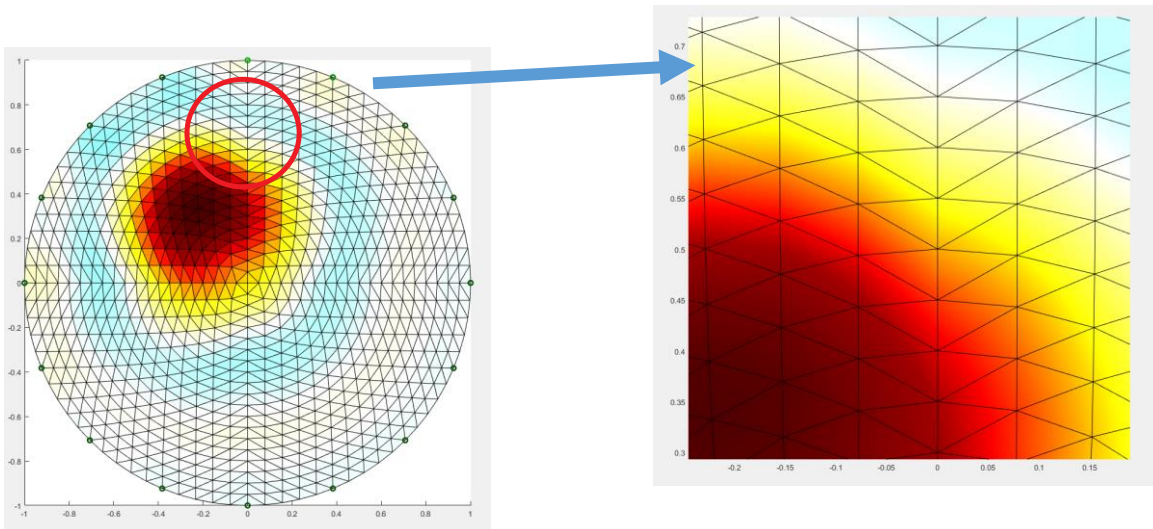


Figure 18. FEM with the target at the left upper side and its zoomed version

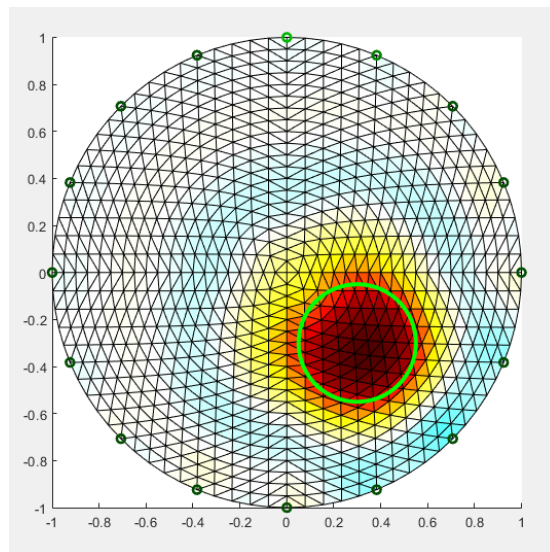


Figure 19. Target reconstruction image with actual target side with the green circle

The images produced by the neural network at the testing phase are shown in the Figure 4.6



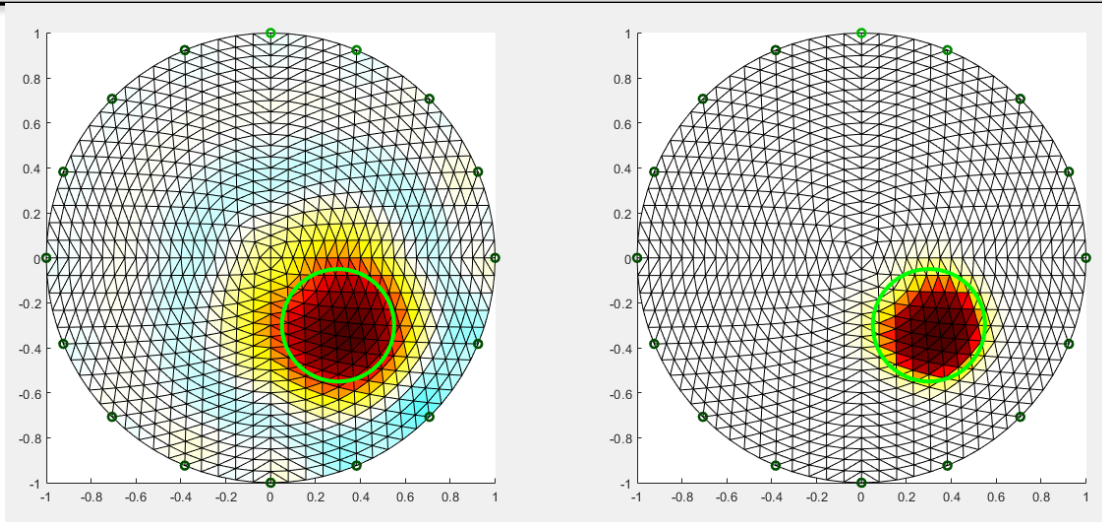


Figure 20. Left: reconstructed image with the target at the center-right down, Right: the resultant image of the actual result after passing through the ANN

The method has also been applied at the half FEM to work at the multi targets in the phantom. Figure 21 and 22.

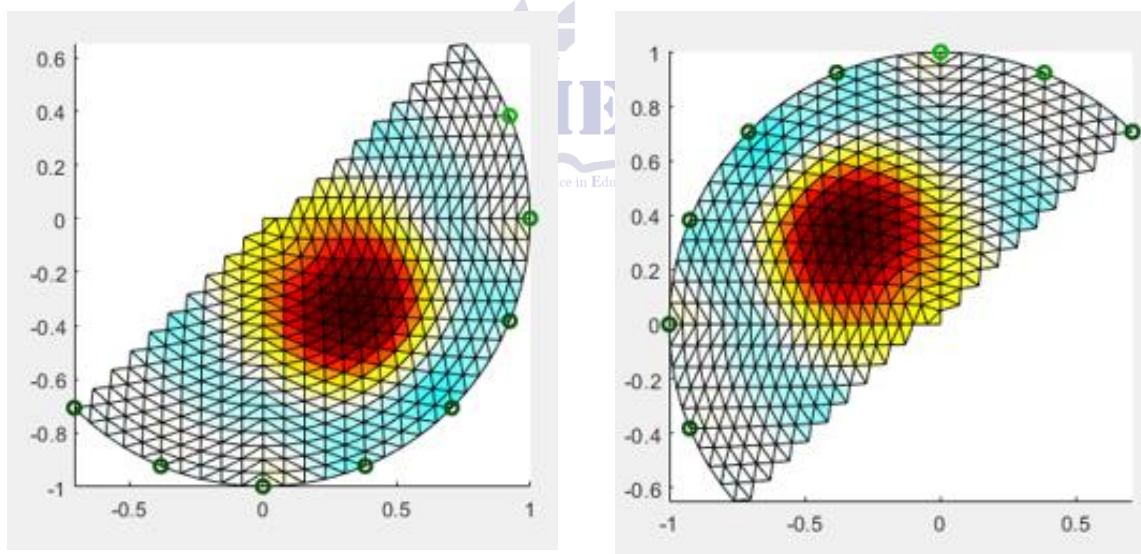


Figure 21. The broken FEM with two target to analyze the target in FEM

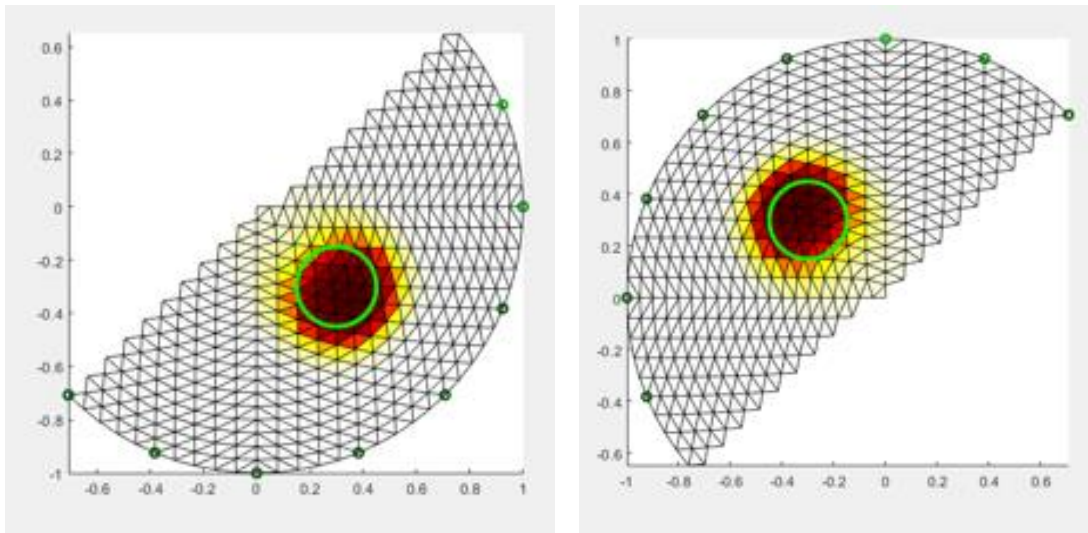


Figure 22 The reconstructed image from the ANN

4. Conclusion

Image reconstruction was performed based on a 2D model, with future work focusing on extending the approach to a 3D model in order to extract a deeper understanding of the system's characteristics. In 1D or 2D models, image signals can be either raw or

filtered. The findings from this study demonstrate that images can be transformed into high-resolution (HR) images, enabling detailed analysis of internal targets in terms of shape, length, and location. The results obtained from this research are shown to be accurate and effective, as illustrated in Figure 23.

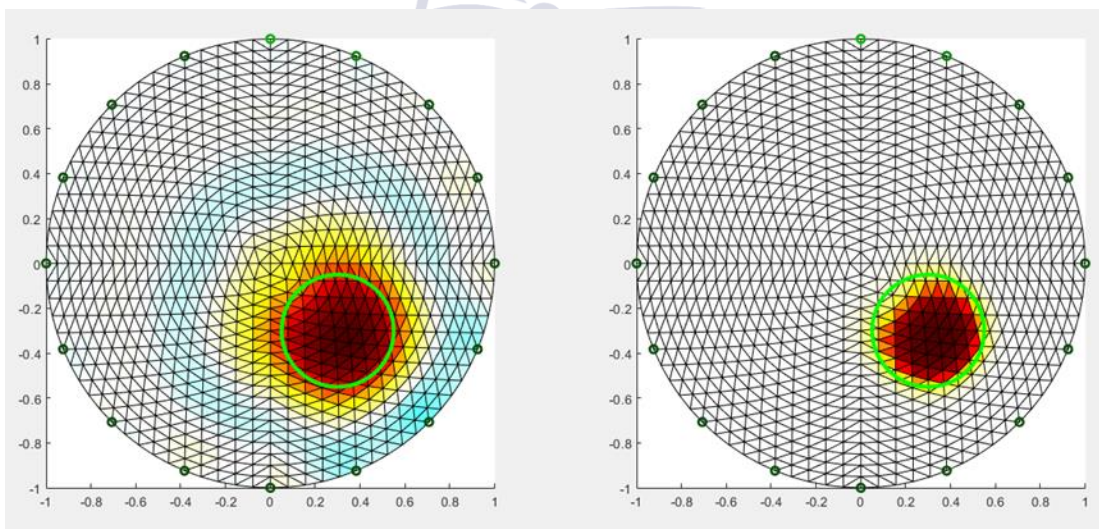


Figure 23. Reconstructed image on left with the ANN image on the right

From Figure 23., it is evident that the left image represents the reconstructed image produced by EIDORS, based on voltage and current measurements at the boundary of the phantom object. The right-hand side image is the result of

applying the artificial neural network (ANN) technique to the raw image without any prior signal processing. Although the results showed minimal differences when using pre-processing techniques, employing pre-processing methods could enhance

the results further. Filters and noise-removal techniques are useful for improving the quality of the reconstructed images. HR image techniques typically involve pre-processing steps such as filtering, feature extraction, transformation, and analysis.

In this research, post-processing was applied to the reconstructed images, with the results derived from the raw dataset signal. The dataset collected from EIDORS will be further enhanced by constructing the phantom object, offering a practical solution to the system. In this context, the phantom targets can be altered in terms of shape, location, and real-time noise conditions. Real-time phantom noise can be addressed through the application mode to improve image accuracy and reliability.

REFERENCES

- [1] A. Adler and W. R. Lionheart, "Uses and abuses of EIDORS: an extensible software base for EIT," *Physiological measurement*, vol. 27, no. 5, p. S25, 2006.
- [2] S. L. Brooks, "Computed tomography," *Dental Clinics of North America*, vol. 37, no. 4, pp. 575-590, 1993.
- [3] L. Borcea, "Electrical impedance tomography," *Inverse problems*, vol. 18, no. 6, p. R99, 2002.
- [4] C. Mittelstädt, T. Mattulat, T. Seefeld, and M. Kogel-Hollacher, "Novel approach for weld depth determination using optical coherence tomography measurement in laser deep penetration welding of aluminum and steel," *Journal of Laser Applications*, vol. 31, no. 2, 2019.
- [5] B. Yegnanarayana, *Artificial neural networks*. PHI Learning Pvt. Ltd., 2009.
- [6] S.-C. Wang, *Interdisciplinary computing in Java programming*. Springer Science & Business Media, 2003.
- [7] L. O. Hall, A. M. Bensaid, L. P. Clarke, R. P. Velthuizen, M. S. Silbiger, and J. C. Bezdek, "A comparison of neural network and fuzzy clustering techniques in segmenting magnetic resonance images of the brain," *IEEE transactions on neural networks*, vol. 3, no. 5, pp. 672-682, 1992.
- [8] E. M. Izhikevich, "Resonate-and-fire neurons," *Neural networks*, vol. 14, no. 6-7, pp. 883-894, 2001.
- [9] B. Ibarz, J. M. Casado, and M. A. Sanjuán, "Map-based models in neuronal dynamics," *Physics reports*, vol. 501, no. 1-2, pp. 1-74, 2011.
- [10] E. M. Izhikevich, "Which model to use for cortical spiking neurons?," *IEEE transactions on neural networks*, vol. 15, no. 5, pp. 1063-1070, 2004.
- [11] I. Kanellopoulos and G. G. Wilkinson, "Strategies and best practice for neural network image classification," *International Journal of Remote Sensing*, vol. 18, no. 4, pp. 711-725, 1997.
- [12] Q. Marashdeh, W. Warsito, L. Fan, and F. Teixeira, "A nonlinear image reconstruction technique for ECT using a combined neural network approach," *Measurement Science and Technology*, vol. 17, no. 8, p. 2097, 2006.
- [13] C. Li, J. Guo, F. Porikli, and Y. Pang, "LightenNet: A convolutional neural network for weakly illuminated image enhancement," *Pattern recognition letters*, vol. 104, pp. 15-22, 2018.
- [14] R. Féraud and F. Clérot, "A methodology to explain neural network classification," *Neural networks*, vol. 15, no. 2, pp. 237-246, 2002.
- [15] A. Adler and R. Guardo, "A neural network image reconstruction technique for electrical impedance tomography," *IEEE Transactions on Medical Imaging*, vol. 13, no. 4, pp. 594-600, 1994.
- [16] S.-W. Fu, T.-y. Hu, Y. Tsao, and X. Lu, "Complex spectrogram enhancement by convolutional neural network with multi-metrics learning," in *2017 IEEE 27th international workshop on machine learning for signal processing (MLSP)*, 2017: IEEE, pp. 1-6.
- [17] S. Sharma, S. Sharma, and A. Athaiya, "Activation functions in neural networks," *Towards Data Sci*, vol. 6, no. 12, pp. 310-316, 2017.

- [18] H. Pratiwi et al., "Sigmoid activation function in selecting the best model of artificial neural networks," in *Journal of Physics: Conference Series*, 2020, vol. 1471, no. 1: IOP Publishing, p. 012010.
- [19] S. Narayan, "The generalized sigmoid activation function: Competitive supervised learning," *Information sciences*, vol. 99, no. 1-2, pp. 69-82, 1997.
- [20] R. Alkhatib, "Artificial Neural Network Activation Functions in Exact Analytical Form (Heaviside, ReLU, PReLU, ELU, SELU, ELiSH)," 2021.
- [21] E. Özçağ, I. Ege, and H. Gürçay, "On powers of the Heaviside function for negative integers," *Journal of mathematical analysis and applications*, vol. 326, no. 1, pp. 101-107, 2007.
- [22] M. Cheney, D. Isaacson, and J. C. Newell, "Electrical impedance tomography," *SIAM review*, vol. 41, no. 1, pp. 85-101, 1999.
- [23] M. Dodd and J. L. Mueller, "A real-time D-bar algorithm for 2-D electrical impedance tomography data," *Inverse problems and imaging (Springfield, Mo.)*, vol. 8, no. 4, p. 1013, 2014.
- [24] A. Hauptmann, V. Kolehmainen, N. M. Mach, T. Savolainen, A. Seppänen, and S. Siltanen, "Open 2D electrical impedance tomography data archive," *arXiv preprint arXiv:1704.01178*, 2017.
- [25] Z. Lin et al., "Neural network-based supervised descent method for 2D electrical impedance tomography," *Physiological measurement*, vol. 41, no. 7, p. 074003, 2020.
- [26] V. Cherepenin et al., "A 3D electrical impedance tomography (EIT) system for breast cancer detection," *Physiological measurement*, vol. 22, no. 1, p. 9, 2001.
- [27] G. González, J. Huttunen, V. Kolehmainen, A. Seppänen, and M. Vauhkonen, "Experimental evaluation of 3D electrical impedance tomography with total variation prior," *Inverse Problems in Science and Engineering*, vol. 24, no. 8, pp. 1411-1431, 2016.
- [28] P. Metherall, D. C. Barber, R. H. Smallwood, and B. H. Brown, "Three-dimensional electrical impedance tomography," *Nature*, vol. 380, no. 6574, pp. 509-512, 1996.
- [29] M. Vauhkonen, W. R. Lionheart, L. M. Heikkinen, P. J. Vauhkonen, and J. P. J. P. m. Kaipio, "A MATLAB package for the EIDORS project to reconstruct two-dimensional EIT images," vol. 22, no. 1, p. 107, 2001.
- [30] A. Adler et al., "EIDORS Version 3.9," in *Proc. 18th Int. Conf. on Biomed. Applications of EIT, 2017: Thayer School of Engineering at Dartmouth*.
- [31] V. Sarode, P. M. Chimurkar, and A. N. Cheeran, "Electrical impedance tomography using EIDORS in a closed phantom," *International Journal of Computer Applications*, vol. 48, no. 19, pp. 975-888, 2012.
- [32] S. C. Park, M. K. Park, and M. G. Kang, "Super-resolution image reconstruction: a technical overview," *IEEE signal processing magazine*, vol. 20, no. 3, pp. 21-36, 2003.
- [33] L. Wald, "Quality of high resolution synthesised images: Is there a simple criterion?," in *Third conference" Fusion of Earth data: merging point measurements, raster maps and remotely sensed images"*, 2000: SEE/URISCA, pp. 99-103.
- [34] C. A. Segall, R. Molina, and A. K. Katsaggelos, "High-resolution images from low-resolution compressed video," *IEEE signal processing magazine*, vol. 20, no. 3, pp. 37-48, 2003.
- [35] K. M. Buddhiraju and I. A. Rizvi, "Comparison of CBF, ANN and SVM classifiers for object based classification of high resolution satellite images," in *2010 IEEE international geoscience and remote sensing symposium, 2010: IEEE*, pp. 40-43.
- [36] S. Shrestha, Z. Bochenek, and C. J. E. e. Smith, "Extreme Learning Machine for classification of high resolution remote sensing images and its comparison with traditional Artificial Neural Networks (ANN)," vol. 13, no. 2, p. 49, 2014.

- [37] A. Wakatani, "Digital watermarking for ROI medical images by using compressed signature image," in Proceedings of the 35th annual Hawaii international conference on system sciences, 2002: IEEE, pp. 2043-2048.
- [38] B. H. J. Lee, S. Jung, and V. J. F. G. C. S. Chang, "Clustering learning model of CCTV image pattern for producing road hazard meteorological information," *Future Generation Computer Systems*, vol. 86, pp. 1338-1350, 2018.
- [39] A. Miller, B. J. M. Blott, B. Engineering, and Computing, "Review of neural network applications in medical imaging and signal processing," vol. 30, no. 5, pp. 449-464, 1992.
- [40] W. Gobel and F. Helmchen, "In vivo calcium imaging of neural network function," *Physiology*, vol. 22, no. 6, pp. 358-365, 2007.
- [41] K. H. Jin, M. T. McCann, E. Froustey, and M. Unser, "Deep convolutional neural network for inverse problems in imaging," *IEEE transactions on image processing*, vol. 26, no. 9, pp. 4509-4522, 2017.
- [42] S. J. Hamilton and A. Hauptmann, "Deep D-bar: Real-time electrical impedance tomography imaging with deep neural networks," *IEEE Transactions on Medical Imaging*, vol. 37, no. 10, pp. 2367-2377, 2018.
- [43] H. Park, K. Park, S. Mo, and J. Kim, "Deep neural network based electrical impedance tomographic sensing methodology for large-area robotic tactile sensing," *IEEE Transactions on Robotics*, vol. 37, no. 5, pp. 1570-1583, 2021.
- [44] B. B. Atitallah et al., "Hand sign recognition system based on EIT imaging and robust CNN classification," *IEEE Sensors Journal*, vol. 22, no. 2, pp. 1729-1737, 2021.
- [45] X. Li et al., "One-dimensional convolutional neural network (1D-CNN) image reconstruction for electrical impedance tomography," *Review of scientific instruments*, vol. 91, no. 12, 2020.
- [46] E. Ratajewicz-Mikolajczak, G. Shirkoohi, and J. Sikora, "Two ANN reconstruction methods for electrical impedance tomography," *IEEE transactions on magnetics*, vol. 34, no. 5, pp. 2964-2967, 1998.
- [47] M. Vauhkonen, W. R. Lionheart, L. M. Heikkinen, P. J. Vauhkonen, and J. P. Kaipio, "A MATLAB package for the EIDORS project to reconstruct two-dimensional EIT images," *Physiological measurement*, vol. 22, no. 1, p. 107, 2001.
- [48] A. Adler and W. R. Lionheart, "EIDORS: Towards a community-based extensible software base for EIT," in Proceedings of the 6th Conference on Biomedical Applications of Electrical Impedance Tomography, London, 2005.
- [49] T. K. Bera and J. Nagaraju, "Studies and evaluation of EIT image reconstruction in EIDORS with simulated boundary data," in Proceedings of the Second International Conference on Soft Computing for Problem Solving (SocProS 2012), December 28-30, 2012, 2014: Springer, pp. 1573-1581.
- [50] G. Dong et al., "The comparison between FVM and FEM for EIT forward problem," *IEEE transactions on magnetics*, vol. 41, no. 5, pp. 1468-1471, 2005.
- [51] P. Wang, H.-l. Li, L.-l. Xie, and Y.-c. Sun, "The implementation of FEM and RBF neural network in EIT," in 2009 Second International Conference on Intelligent Networks and Intelligent Systems, 2009: IEEE, pp. 66-69.
- [52] F. Casadei, E. Gabellini, G. Fotia, F. Maggio, and A. Quarteroni, "A mortar spectral/finite element method for complex 2D and 3D elastodynamic problems," *Computer methods in applied mechanics and engineering*, vol. 191, no. 45, pp. 5119-5148, 2002.
- [53] X. Fernández-Fuentes, D. Mera, A. Gómez, and I. Vidal-Franco, "Towards a fast and accurate eit inverse problem solver: A machine learning approach," *Electronics*, vol. 7, no. 12, p. 422, 2018.

- [54] B. Graham and A. Adler, "A nodal Jacobian inverse solver for reduced complexity EIT reconstructions," *Int. J. Inf. Syst. Sci.*, vol. 2, no. 4, pp. 453-468, 2006.
- [55] H. Gagnon, M. Cousineau, A. Adler, and A. E. Hartinger, "A resistive mesh phantom for assessing the performance of EIT systems," *IEEE transactions on biomedical engineering*, vol. 57, no. 9, pp. 2257-2266, 2010.
- [56] A. Adler et al., "GREIT: a unified approach to 2D linear EIT reconstruction of lung images," *Physiological measurement*, vol. 30, no. 6, p. S35, 2009.
- [57] B. Graham and A. Adler, "Electrode placement configurations for 3D EIT," *Physiological measurement*, vol. 28, no. 7, p. S29, 2007.
- [58] F. Locment, T. Henneron, E. Semail, and F. Piriou, "Using 3D-FEM for design of an axial flux seven-phase machine," in *Symposium On Electric and Magnetic Fields (EMF2006)*, Aussois (France), 2006.
- [59] M. Soleimani, C. Gómez-Laberge, and A. Adler, "Imaging of conductivity changes and electrode movement in EIT," *Physiological measurement*, vol. 27, no. 5, p. S103, 2006.
- [60] L.-J. Xie, J. Schmidt, C. Schmidt, and F. Biesinger, "2D FEM estimate of tool wear in turning operation," *Wear*, vol. 258, no. 10, pp. 1479-1490, 2005.
- [61] M. T. Simons et al., "Electromagnetically Induced Transparency (EIT) and Autler-Townes (AT) splitting in the presence of band-limited white Gaussian noise," *Journal of Applied Physics*, vol. 123, no. 20, 2018.
- [62] A. Dupré, G. Ricciardi, S. Bourennane, and S. Mylvaganam, "Identification of flow regimes using raw EIT measurements," in *8th World Congress on Industrial Process Tomography WCIPT8*, 2016.
- [63] D. Nguyen, C. Jin, A. Thiagalingam, and A. McEwan, "A review on electrical impedance tomography for pulmonary perfusion imaging," *Physiological measurement*, vol. 33, no. 5, p. 695, 2012.
- [64] K. Arjun and K. Aneesh, "Modelling studies by application of artificial neural network using matlab," *Journal of Engineering Science and Technology*, vol. 10, no. 10, pp. 1477-1486, 2015.
- [65] M. T. Hagan, H. B. Demuth, and M. Beale, *Neural network design*. PWS Publishing Co., 1997.
- [66] T. Zhong and X. Tao, "Application and Simulation of Matlab Neural Network Tool NNTool," *Computer and Modernization*, vol. 208, no. 12, p. 44, 2012.
- [67] S.-W. Huang, H.-M. Cheng, and S.-F. Lin, "Improved imaging resolution of electrical impedance tomography using artificial neural networks for image reconstruction," in *2019 41st Annual International Conference of the IEEE Engineering in Medicine and Biology Society (EMBC)*, 2019: IEEE, pp. 1551-1554.
- [68] F. H.-F. Leung, H.-K. Lam, S.-H. Ling, and P. K.-S. Tam, "Tuning of the structure and parameters of a neural network using an improved genetic algorithm," *IEEE transactions on neural networks*, vol. 14, no. 1, pp. 79-88, 2003.
- [69] L. K. Hansen, P. J. I. t. o. p. a. Salamon, and m. intelligence, "Neural network ensembles," vol. 12, no. 10, pp. 993-1001, 1990.
- [70] S. Han, J. Pool, J. Tran, and W. Dally, "Learning both weights and connections for efficient neural network," *Advances in neural information processing systems*, vol. 28, 2015.
- [71] E. Gelenbe, "Stability of the random neural network model," *Neural computation*, vol. 2, no. 2, pp. 239-247, 1990.
- [72] A. Adler, A. Borsic, N. Polydorides, and W. R. Lionheart, "Simple FEMs aren't as good as we thought: experiences developing EIDORS v3.3," 2008.